Title	Chondrocytes derived from mesenchymal stromal cells and induced pluripotent cells of patients with familial osteochondritis dissecans exhibit an endoplasmic reticulum stress response and defective matrix assembly
Author(s)	Xu, Maojia; Stattin, Eva-Lena; Shaw, Georgina; Heinegård, Dick; Sullivan, Gareth; Wilmut, Ian; Colman, Alan; Önnerfjord, Patrik; Khabut, Areej; Aspberg, Anders; Dockery, Peter; Hardingham, Timothy; Murphy, Mary; Barry, Frank
Publication Date	2016-07-07
Publication Information	Xu, Maojia; Stattin, Eva-Lena; Shaw, Georgina; Heinegård, Dick; Sullivan, Gareth; Wilmut, Ian; Colman, Alan; Önnerfjord, Patrik; Khabut, Areej; Aspberg, Anders; Dockery, Peter; Hardingham, Timothy; Murphy, Mary; Barry, Frank (2016). Chondrocytes derived from mesenchymal stromal cells and induced pluripotent cells of patients with familial osteochondritis dissecans exhibit an endoplasmic reticulum stress response and defective matrix assembly. STEM CELLS Translational Medicine 5 (9), 1171-1181, doi: 10.5966/sctm.2015-0384
Publisher	Wiley
Link to publisher's version	https://doi.org/10.5966/sctm.2015-0384
Item record	http://hdl.handle.net/10379/15186
DOI	http://dx.doi.org/10.5966/sctm.2015-0384

Chondrocytes derived from mesenchymal stromal cells and induced pluripotent cells of patients with familial osteochondritis dissecans exhibit an ER stress response and defective matrix assembly

Maojia Xu[1], Eva-Lena Stattin[2], Georgina Shaw[1], Dick Heinegård[3†], Gareth Sullivan[4], Ian Wilmut[5], Alan Colman[6], Patrik Önnerfjord[3], Areej Khabut[3], Anders Aspberg[3], Peter Dockery[7], Timothy Hardingham[8], Mary Murphy[1], Frank Barry[1]

[1]Regenerative Medicine Institute (REMEDI), National University of Ireland Galway, Galway, Ireland; [2]Department of Immunology, Genetics and Pathology, Science for Life Laboratory, Uppsala University, 75185 Uppsala, Sweden; [3]Department of Clinical Sciences, Rheumatology and Molecular Skeletal Biology, Lund University, 22184 Lund, Sweden; [4]Norwegian Center for Stem Cell Research, PO Box 1112 Blindern, 0317 Oslo, Norway; [5]MRC Centre for Regenerative Medicine, University of Edinburgh, Edinburgh EH16 4SB, UK; [6]A*STAR Institute of Medical Biology, 138648 Singapore; [7]Anatomy, School of Medicine, National University of Ireland Galway, Galway, Ireland. [8]Welcome Trust Centre for Cell-Matrix Research, Faculty of Life Sciences University of Manchester, Manchester M13 9PT UK

†-Author deceased

Author's contribution(s)

Maojia Xu: Conception and design, collection and/or assembly of data, data analysis and interpretation, manuscript writing

Eva-Lena Stattin: Provision of study material or patients, manuscript writing

Georgina Shaw: Conception and design, collection and/or assembly of data, data analysis and interpretation, manuscript writing

Dick Heinegård: Conception and design, data analysis and interpretation

Gareth Sullivan: Provision of study material or patients

Ian Wilmut: Provision of study material or patients

Alan Colman: Conception and design,

Patrik Önnerfjord: Collection and/or assembly of data, data analysis and interpretation, manuscript writing

Areej Khabut: Collection and/or assembly of data, data analysis and interpretation, manuscript writing

Anders Aspberg: Data analysis and interpretation, manuscript writing

Peter Dockery: Data analysis and interpretation, manuscript writing

Timothy Hardingham: Data analysis and interpretation, manuscript writing

Mary Murphy: Conception and design, Data analysis and interpretation, Manuscript writing

Frank Barry: Conception and design, Data analysis and interpretation, Manuscript writing, Final approval of manuscript

Corresponding author: Frank Barry PhD

The Regenerative Medicine Institute (REMEDI), National University of Ireland Galway, Galway, Ireland

t: +353 (0)91 49 5108; f: +353 (0)91 49 5547

Email: frank.barry@nuigalway.ie

The work presented here is supported by Science foundation Ireland (SFI) grant (09/SRC/B1794), Irish Research Council (IRC) grant (GOIPG/2014/96) and the European Union's Seventh Framework Programme grant (223298).

Key words: Osteoarthritis, Familial osteochondritis dissecans, Mesenchymal stromal cells, Induced pluripotent stem cells, Stem cell disease models, Cellular pathology, Aggrecan mutation, Endoplasmic reticulum stress

Abstract

Familial osteochondritis dissecans (FOCD) is an inherited skeletal defect characterized by the development of large cartilage lesions in multiple joints, short stature and the early onset of severe osteoarthritis (OA). It is associated with a heterozygous mutation in the ACAN gene, resulting in a Val-Met replacement in the C-type lectin domain of aggrecan. To understand the cellular pathogenesis of this condition, we studied the chondrogenic differentiation of patient bone marrow mesenchymal stromal cells (BM-MSCs). We also looked at cartilage derived from induced pluripotent stem cells (iPSCs) generated from patient fibroblasts. Our results revealed several characteristics of the differentiated chondrocytres that help to explain the disease phenotype and the susceptibility to cartilage injury. Firstly, patient chondrogenic pellets had poor structural integrity but were rich in glycosaminoglycan. Secondly, it was evident that large amounts of aggrecan accumulated within the endoplasmic reticulum of chondrocytes differentiated from both BM-MSCs and from iPSCs. In turn there was a marked absence of aggrecan in the extracellular matrix (ECM). Thirdly, it was evident that matrix synthesis and assembly were globally disregulated. These results highlight some of the abnormal aspects of chondrogenesis in these patient cells and help to explain the underlying cellular pathology. The results suggest that FOCD is a chondrocyte aggrecanosis with associated matrix disregulation. The work provides a new vitro model of OA and cartilage degeneration based on the use of iPSCs and highlights how new insights into disease phenotype and pathogenesis can be uncovered by studying differentiation of patient stem cells.

Introduction

Mesenchymal stromal cells (MSCs) from bone marrow and other tissues have the capacity to differentiate to chondrocytes. The differentiated cell phenotype has been well characterized and shares many cellular and extracellular matrix (ECM) features of primary chondrocytes isolated from articular cartilage. MSCs can also be prepared from induced pluripotent stem cells iPSCs) generated from dermal fibroblasts or other cells and can also form chondrocytes. Our objective in this study was to assess whether analysis of the differentiated phenotype in cells from patients with osteoarthritis (OA) would shed light on the cellular pathology of the disease. Idiopathic OA occurs widely and has a broad spectrum of symptoms and probably a broad spectrum of causation, making interpretation of results in studies such as this potentially difficult. We therefore selected a monogenic disease, familial osteochondritis dissecans (FOCD), associated with a known single mutation and characterized by the development of early and severe OA. We isolated MSCs and generated iPSCs from FOCD patients and assessed their chondrogenic differentiation in an attempt to shed light on the cellular pathology that gives to the unstable and rapidly degenerating articular cartilage in these patients.

Osteochondritis dissecans (OCD) is a serious disease of joints characterized by separation of articular cartilage from subchondral bone [1, 2]. The most commonly affected joints are the knee, elbow and ankle, but other joints may be involved [3-7]. Symptoms include pain on activity, effusion, crepitation and limited range of movement [8]. Development of degenerative osteoarthritis (OA) is common in patients with OCD [9]. FOCD has been reported on a number of occasions where an underlying hereditary factor exists [10-13]. This study focuses on a family from Northern Sweden, first reported by Stougaard in 1964 [13], with FOCD (referred to as FOCD-NS) inherited in an autosomal dominant pattern [12]. The results of a genome-wide scan and DNA sequencing showed that all affected family members

bear a heterozygous G-A mutation in aggrecan exon 17, which results in a Val-Met amino acid replacement (V2303M) in the G3 aggrecan C-type lectin domain (CLD) [14].

Aggrecan, a major proteoglycan of articular cartilage produced by chondrocytes, has a large protein core richly substituted with sulfated glycosaminoglycan (GAG) chains. The aggrecan protein core follows the secretory pathway within the chondrocyte; it is made in the rough endoplasmic reticulum (rER) and then translocated to the Golgi for GAG chain synthesis and sulfation, prior to secretion to the extracellular matrix (ECM) [15]. The unique structure, its high concentration within the ECM, and its ability to form a supermolecular complex with hyaluronan and bind to other matrix proteins all profoundly influence the biomechanical properties of the tissue [16]. Deletion of aggrecan G3 domain in a mutant chick (nanomelia) was found to block aggrecan secretion from chondrocytes [17]. Further evidence using aggrecan synthesised with no naturally folded G3 also indicated a role for this domain in intracellular trafficking and secretion.[18]. An important function of the G3 CLD domain is binding to tenascin-C, tenascin-R, fibulin-1, and fibulin-2 in cartilage ECM [19] and human aggrecan constructs carrying the V2303M mutation were shown to have diminished interactions with these binding partners [14].

We cultured mesenchymal stromal cells (MSCs) from bone marrow (BM) of an FOCD-NS patient and induced them to differentiate into chondrocytes [20]. Analysis of the phenotype of differentiated cells revealed an abnormal intracellular processing pathway and limited extracellular distribution of aggrecan. Furthermore, we showed that the mutated aggrecan caused morphological changes in the rER within the chondrocytes. Our experiments suggested a cellular pathology of FOCD-NS with misfolded aggrecan accumulating inside the rER, resulting in ER stress and leading to a deficiency of cell function in protein secretion. As a consequence, there was defective development of the cartilaginous ECM, with a distinctly abnormal composition of key proteins and proteoglycans. This suggested that, in

addition to defective aggrecan processing, synthesis and assembly of the entire ECM is impaired.

To further extend our observations, we prepared patient-specific induced pluripotent stem cells (iPSCs) with successful reprogramming of skin fibroblasts from two FOCD-NS patients. By exploiting the potential of iPSCs when implanted in vivo to form teratomas with tissues from all three germ layers, including cartilage, we were able to show that the same disease phenotype was recapitulated in the iPSC-derived cartilage within teratomas. These results provide new insight into the cellular phenotype of FOCD and demonstrate for the first time a disease model of a monogenic OA based on patient specific iPSCs.

Materials and Methods

Ethical approvals

All animal experimentation complied with institutional guidelines and had ethical approval from the Animal Care Research Ethics Committee at the National University of Ireland (NUI) Galway (05/Jun/03). MSCs were isolated from BM harvested from the iliac crest of a healthy donor with approval from both the NUI Galway Research Ethical Committee (08/May/14) and Galway University Hospitals Clinical Research Ethics Committee (2/08). The ethical approval for harvesting skin tissue and BM from FOCD-NS patients for primary cell culture and stem cell study were issued by the Regional Ethical Review Board in Umeå, Sweden, Dnr 2010/408-31M, and 2007/109M (01-244).

Tissue samples

A BM sample was obtained from a 49-year-old male FOCD-NS patient during joint replacement surgery and normal human BM-MSC (053) were isolated from a 33-year-old male healthy donor. Dermal fibroblasts were obtained from a 25-year-old son (FOCD-NS1)

and 49year-old mother (FOCD-NS2) for generation of patient-derived iPSC. An iPSC line (33D-6) from a healthy donor (56-year-old male) was obtained from Dr Gareth Sullivan (University of Edinburgh, UK) [21].

Isolation and characterization of MSCs from patient and control marrow

BM-MSCs were isolated and characterized (adipogenesis and osteogenesis) as previously described [20]. To assess positive and negative surface markers of BM-MSCs, the Human MSC Analysis Kit (BD Bioscience) was used according to the manufacturer's protocol. Data was analysed by FlowJo 6.0.

Chondrogenesis of BM-MSCs

To detect the disease phenotypes, chondrogenesis of BM-MSCs was performed using micropellet culture as described previously [20]. As the brief centrifugation step associated with micropellet formation affected the structure of pellets derived from patient cells, a modified high cell density micromass method was performed as previously described [22, 23]. Briefly, 2 X 10^5 of BM-MSCs in 10 µl was incubated at 37°C for 2 hours in low adherent round bottom 96-well plates (Sigma). 200µl of MSC maintenance medium was then added into each well, followed by overnight incubation. Medium was replaced by chondrogenic medium with 10 ng/ml TGF-β3 [20] at day 2 and was changed at every second day. Micropellets and micromass cultures were harvested at different time points.

Sulphated glycosaminoglycan (GAG) and DNA quantification

For quantification of GAG, dimethylmethylene blue (DMMB) was performed as described previously [20]. DNA was measured by PicoGreen® dsDNA assay kit (Invitrogen), according to the manufacturer's protocol. To assess the chondrogenic capability of control and FOCD-NS cells, the ratio of GAG to DNA was calculated.

Histological and immunohistochemical analysis of chondrogenic pellets

Samples were processed as previously described [20]. For detection of GAG, sections were stained with 0.5% toluidine blue (pH8) for 5 minutes at 60°C. Immuno-staining was performed to investigate the distribution of ECM proteins (collagen type II and aggrecan) and co-localization of aggrecan and glucose regulated protein (GRP78) in chondrogenic pellets and cultures. Detailed experimental procedures can be found in supplemental data.

Brightfield and confocal microscopy were used to examine the immunohistochemical and immunofluorescence stained specimens. The magnified images for detection of cell morphology and ECM distribution were created by ImageJ.

Transmission electron microscopy (TEM)

To analyse ECM formation and ultrastructure of ER, day 56 micromass cultures were processed for TEM examination as previously described [24] Samples were examined using the Hitachi H7000 transmission electron microscope.

To estimate the volume fraction (Vv) of rER to cell cytoplasm, a systematic random sampling protocol was adopted. This consisted of a series of images (10) taken across the pellet at an initial magnification of 3,000X. Three further images were taken from each field at a magnification 10,000X. Simple point counting methods were used to estimate cellular composition [25].

Mass spectrometry

For sample preparation, a modified protocol for extracting peptides from chondrogenic pellets derived from BM-MSCs was performed based on a previous description [26]. Detailed experimental procedures can be found in supplemental data. Each sample was run in technical duplicate. The measured peptide transitions are listed in Supplemental Table 3.

Three to six transitions for each peptide were measured in a scheduled multiple reaction monitoring method [26]. Briefly, the amount of each protein was normalized by the pellet volume. The mean ratios of ECM proteins between FOCD and control BM-MSC derived pellets were calculated.

iPSC generation and characterization

For reprogramming, isolated skin fibroblasts from two patients (FOCD-NS1 and FOCD-NS2) were transfected by retrovirus containing the four Yamanaka reprogramming factors as described previously [27]. Resulting iPSC colonies were expanded. To assess the pluripotency of these iPSCs, semiquantitative RT-PCR, immunocytochemistry, flow cytometry, teratoma formation *in vivo*, karyotype analysis and mutation verification were performed. See supplemental data for detailed protocols.

Verification of disease phenotype in iPSC-derived cartilage

Cartilaginous nodules formed in teratoma derived from one control and four FOCD-NS iPSC lines were studied. To identify cartilage tissues in teratoma sections, samples were stained with 0.02% fast green solution followed by 0.1% safranin-O solution. Cartilage tissue appeared red and non-cartilage tissues showed green. To study the distribution of aggrecan protein in these tissue, immunohistochemical staining was performed. Detailed experimental procedures can be found in supplemental data.

Results

FOCD-NS MSC characterization

MSCs isolated from bone marrow of a FOCD-NS patient were morphologically similar to cells from a healthy donor (Figure 1A), with similar cell surface phenotype. Both control and FOCD-NS BM-MSCs were positive for CD90/73/105 (Figure 1B). Combined levels of

hematopoietic cell markers CD11b/34/19/45 and HLA-Dr were substantially lower in patient cells (0.149%) compared to controls (9.17%, Figure 1B). The patient marrow appeared to have a high fat content and yielded low numbers of mononuclear cells. Both patient and control MSCs were assessed for multipotency using trilineage differentiation tests. Both populations showed a capacity to differentiate into osteoblasts and adipocytes (Figure 1C). In contrast, there were marked differences between patient and control cells in chondrogenic pellet cultures. Both MSC populations readily formed white cartilaginous pellets, but patient samples had an irregular discoid morphology (Figure 2A and B). Patient pellets (diameter 1.5-2mm) were larger with a rough surface compared to the smooth glistening surface of control pellets (diameter 1-1.5mm). In addition, there was greater GAG staining in the FOCD-NS pellets (Figure 2B).

Characterization of chondrogenic cultures

Immunohistochemical staining of chondrogenic pellets was performed using an antibody specific for the interglobular domain (IGD) of aggrecan. In control pellets, aggrecan was clearly discernible within the chondrocytes and throughout the matrix; staining was primarily intracellular at early time points and progressed through pericellular localisation evident from day 5 to intraterritorial distribution by day 14 (Figure 2C, left panel). In contrast, in the patient pellets aggrecan staining was predominantly cellular or pericellular with minimal territorial or intraterritorial matrix staining at 14 days. At earlier times, some aggrecan was detected in the extracellular matrix, perhaps reflecting the heterozygous nature of the FOCD-NS mutation, but this diminished by day 5 in culture (Figure 2C, right panel). This result suggested that the effect of the mutation within the CLD domain was to impede normal processing and stabilization of aggrecan within the ECM.

To allow careful comparison between patient and control cells we used micromass cultures without centrifugation. Micromass culture allows self-assembly of cells at high density into organized aggregates and may allow for better cell-cell contact, thus facilitating chondrogenic differentiation more typically seen during development [22]. To reflect the adult onset of the condition, micromass cultures were maintained for periods of time between 14 and 100 days. Histological analysis showed that patient cells were able to form regular spherical micromass cultures of larger dimension than those derived from control cells (Figure 3A). We carried out co-staining for aggrecan protein and the glucose-regulated protein (GRP78), a rER chaperone [28]. GRP78 resides within the rER and its functions include control of new protein folding and recognition of unfolded or misfolded proteins. Analysis of long term chondrogenic micromass cultures of control cells (Figure 3B) revealed large amounts of aggrecan in the ECM with some intracellular GRP78 staining, indicating aggrecan processing through the ER. There was also some evidence of nascent aggrecan within cells. In stark contrast, patient cultures showed no aggrecan staining in the ECM but rather a distinctly intracellular pattern with a clear co-localization with GRP78. This dramatic difference in patient cells indicated there was an accumulation of aggrecan within the rER and an inability to process and secrete to the ECM (Figure 3B).

Analysis of GAG accumulation in long-term chondrogenic cultures of patient cells was carried out. At early time points, there was 15-fold higher GAG accumulation in FOCD-NS cultures compared to controls (9.5 versus 0.6 μg GAG/pellet, Figure 4A). However, in these cells longer incubation resulted in a decreased GAG content, whereas control cells demonstrated a progressive increase. Measurement of DNA content per pellet showed a higher level in patient cells, suggesting a greater degree of mitotic activity. When GAG was measured as a function of DNA content, patient cells only produced a substantially higher GAG per cell at day 14 and a low ratio of GAG/DNA remained constant throughout the long

term culture of patient cells. Whereas this ratio increased greatly with time in control samples and exceeded that in patient samples at day 35. These results suggested that either GAG synthesis in the patient cells is inhibited in long term cultures, that there is a higher degradative activity, or that chondrogenic differentiation is otherwise delayed or arrested in FOCD-NS cultures (Figure 4A).

Analysis by transmission electron microscopy (TEM) of control pellets showed evidence of long fibrillar bundles in the ECM of day 56 micromass cultures, but little evidence of these in patient samples (Figure 4B and Supplemental Figure 1). A characteristic of the FOCD chondrocytes was rER with physically enlarged surface area (Figure 4B-e). In contrast, the rER in control chondrocytes had a normal appearance (Figure 4B-b). The volume fractions (Vv) of rER to cell cytoplasm in control and FOCD-NS samples indicated that the surface area of rER in patient samples was twice that of control samples (Figure 4C). Immunostaining of micromass pellets from day 42 showed the patient sample had a lower density of collagen type II fibres than found in the control sample (Figure 4D).

Quantitative analysis of ECM proteins

We analyzed the protein, proteoglycan and collagen composition of ECM generated by chondrocytes differentiated from patient marrow-derived MSCs compared to controls. These analyses were performed using guanidinium hydrochloride extracts of pellets and included both intracellular and extracellular components. There were marked differences which pointed to a highly dysregulated matrix assembly in patient cells (Figure 5 and Supplemental Table 3). Firstly, we noted a reduction of approximately 50% in aggrecan content in patient cells, while the hyaluronan proteoglycan link protein was increased approximately 1.7 fold. The peptide analysis used in these measurements did not include the mutated region of the patient aggrecan G3 domain. Nine common small leucine-rich proteoglycans (SLRPs) were

analysed. Of these, asporin (class 1 SLRP), osteoadherin (class 2 SLRP) and mimecan (class 3 SLRP) were dramatically upregulated in patient cells. These three proteins have all been linked to mineralization [29, 30] often seen in OA[31]. The proteoglycans versican and perlecan also clearly increased in patient cultures. Among the glycoproteins analyzed, cartilage oligomeric matrix protein (COMP), fibronectin and tenascin-C were all upregulated dramatically in FOCD-NS, whereas thrombospondin-1 was slightly increased in controls. Examination of collagen fibres contained in the ECM revealed that patient samples had 2-3-fold higher extractable collagen alpha-3 (VI) and collagen alpha-2(XI), than controls. However, the amount of collagen alpha-1(II) chain chondrocalcin and collagen alpha-1(II) chain N-propeptide were similar between the two groups. Among other ECM proteins, we found that cartilage intermediate layer protein-2 (CILP-2) was uniquely present in the patient samples (Supplemental Table 3), matrilin-3 was expressed 6-fold higher in FOCD-NS, and there was no difference between the two groups in the level of dermatopontin.

Generation and characterization of FOCD-NS specific iPSCs

We generated patient-specific iPSCs from dermal fibroblasts from 2 patients, a son aged 25 (FOCD-NS1) and mother aged 49 (FOCD-NS2). Both patients had the heterozygous G-A transition in exon 17 of the ACAN gene. The fibroblasts were transfected by retrovirus encoding OCT4, SOX2, C-MYC and KLF4 and then were cultured in iPSCs maintenance medium supplemented with valproic acid. Mesenchymal to epithelial transition was detected in transfected fibroblasts 6 days after infection (Figure 6A-a) and colonies with morphology typical of human embryonic stem cells (ESCs) appeared around day 14 (Figure 6A-b). These colonies were picked for cell line establishment from day 21 to day 30 (Figure 6A-c). Seven human ESC-like colonies were obtained from FOCD-NS1 fibroblasts and three from FOCD-NS2 fibroblasts. All were successfully expanded in culture. Once the iPSC lines were established, cells were adapted from feeder-dependent to feeder-free culture conditions.

Two colonies with human ESC-like morphology were randomly selected from each patient, and named FOCD-NS1-iPSC-2/30 andFOCD-NS2-iPSC-9/13. A healthy donor iPSC line (33D-6) was generated by the same methodology as a control. Standard G-banding chromosome analysis was performed and showed that the selected FOCD-NS-iPSC lines had a normal karyotype (Figure 6B). The expression of retroviral transgenes (Tg-OCT4/SOX2/ KLF4/C-MYC) and endogenous pluripotency markers was assessed by semi-quantitative RT-PCR, which confirmed that transgenic transcripts were silenced and endogenous OCT4, SOX2 and NANOG were detected in all FOCD-NS-iPSC lines (Figure 6C). It was confirmed that the heterozygous G-A transition in exon 17 of the ACAN gene persisted after reprogramming by DNA sequence analysis (Figure 6D). Moreover, immunostaining confirmed that FOCD-NS-iPSCs expressed OCT4, SOX2, NANOG and the pluripotent-specific surface antigen TRA1-60 (Figure 6E). Flow cytometry indicated that 97.8-99.8% of the cell population in the FOCD-NS–iPSC lines expressed the surface antigen SSEA4, levels somewhat higher than in the control iPSC line (94%, Figure 6F). To determine pluripotency *in vivo*, four FOCD-NS-iPSC lines and 33D-6 were injected subcutaneously into SCID-Bergin mice. Formed teratomas were observed from week 6 post-injection and were harvested after 2 - 3 months. All cell lines showed the ability to differentiate into different tissues from three germ layers (Figure 6G: Endoderm (glands a-e), Mesoderm (bone (f), muscle (g), gut associated lymphoid tissue (h), fat (i), blood vascular (j)), and Ectoderm (neural rosette (k, o), hair bulb hair follicle (l), squamous epithelium cell (m), pigmented cell (n)).

The iPSC model reproduces the disease phenotype

Cartilage tissues in teratomas generated from the FOCD-NS-iPSC lines were compared to those from control iPSCs. The cartilage was visualized by Safranin-O staining (Figure 7, top panels). To verify whether the FOCD-NS iPSC-derived cartilage reproduced the disease

phenotype, immunohistochemical staining for aggrecan was performed. In control teratoma cartilage, aggrecan was extracellular and distributed evenly in the ECM. In teratoma cartilage from the four FOCD-NS-iPSC lines, aggrecan was found dominantly within chondrocytes and the ECM was largely depleted (Figure 7, mid and bottom panels). Furthermore, cells were densely packed, perhaps reflecting decreased matrix production or delayed differentiation. Histological analysis showed that intercellular accumulation of aggrecan in patient lines occurred at different stages of chondrocytic differentiation, from early resting or proliferating phase to hypertrophic phase (Figure 7, bottom panels).

Discussion

We have characterized MSCs taken from the bone marrow of patients with FOCD-NS, carrying a V2303M mutation compared to MSCs from healthy controls. In terms of analysis of cell surface markers and osteogenic and adipogenic differentiation, MSCs from both groups appeared identical (Figure 1A-C) [32]. As expected, substantial differences were observed in chondrocytes derived from patient compared to control MSCs. Chondrogenic pellets from patient MSCs were irregular, with a “donut” shape rather than a spherical morphology (Figure 2A). It was evident that patient chondrocytes rapidly produced abundant GAG chains attached to aggrecan during processing in the Golgi (Figure 2B) [15]. This may have resulted from expression of the non-mutated allele. In micromass cultures the FOCD-NS chondrocytes formed uniform spheres (Figure 3A), while in conventional pellet cultures they were irregular discoids. This may be a consequence of the inability of the patient cells to resist the mechanical load associated with centrifugation.

Immunostaining showed that aggrecan was clearly distributed throughout the ECM in control chondrocytes but had a sharply cellular distribution in patient chondrocytes, suggesting that in these the processing, assembly and secretion of aggrecan were defective (Figure 2C).

Confocal microscopy confirmed this and also appeared that the ECM of patient chondrocytes was devoid of aggrecan (Figure 3B). Further, we found that intracellular aggrecan was clearly associated with the ER, indicated by co-staining with the ER marker protein GRP78 (Figure 3B). This confirmed a defect in processing of aggrecan associated with retention within the ER and failure to translocate to Golgi and to be secreted. Quantification of GAG and DNA in micromass cultures derived from controls and FOCD-NSs suggested that early intracellular accumulation of aggrecan proteins resulted in enhanced cell proliferation and also reduced chondrogenic capacity (Figure 4A). Further evaluation using TEM confirmed the absence of a fibrillar matrix and the presence of an atypical, diffuse ultrastructure within patient chondrocytes (Figure 4B and Supplemental Figure 1). Physically enlarged rER in patient cells further proved that it was packed with protein products during chondrogenesis (Figure 4B). All these observations pointed towards a failure of FOCD-NS mesenchymal progenitors to assemble aggrecan within the ER and to secrete it from the cell following differentiation. Using peptide-specific mass spectrometric analysis, we analysed ECM proteins to determine how they are differently modulated in patient chondrocytes derived from primary MSCs. There were several striking differences between the patient chondrocytes and those from healthy controls. We found a 50% reduction in aggrecan in patient samples (Figure 5 and Supplemental Table 3), which suggested that the CLD mutation results in attenuated production of aggrecan during the chondrogenic process. Interestingly, versican expression was 6.8 fold higher in patient samples (Figure 5 and Supplemental Table 3). We speculate that this up-regulation may act to compensate for the lack of aggrecan in the ECM or could reflect delayed chondrogenic differentiation. Secondly, a group of proteins associated with cartilage degeneration were highly upregulated in FOCD-NS samples: asporin, mimecan, fibronectin, matrilin-3, COMP, tenascin-C and perlecan (Figure 5 and Supplemental Table 3) [30, 33-39]. This composition of the ECM in FOCD-NS chondrocytes reflects those changes

seen in advanced OA. Interestingly, thrombospondin-1, whose function relates to the restoration of homeostasis in degenerated joints [40], was slightly reduced in FOCD-NS cultures. In addition, comparing other essential components of the ECM between healthy and FOCD-NS samples revealed wide variations in production levels (Figure 5 and Supplemental Table 3). In summary, these results outlined the consequences of early intracellular accumulation of mutated aggrecan, and indicated cartilaginous dysplasia in later chondrogenesis of FOCD-NS samples.

There are two difficulties associated with examination of primary MSCs from patients with FOCD-NS, namely the limited availability of marrow and its abnormal cellularity. Marrow aspirates taken from the patients were white, fatty, and different from healthy marrow. Upon plating, the yield of MSCs was low, although sufficient for the characterization described above. Further characterization required the generation of patient-specific iPSCs. We successfully generated iPSCs from patient fibroblasts (Figure 6) and confirmed that the mutation in exon 17 of the aggrecan gene was preserved (Figure 6D).

We looked in detail at cartilage nodules within teratomas derived from FOCD-NS-iPSCs. Here we found the same disease phenotype observed in chondrogenic cultures of primary MSCs, i.e. rich in GAG but with a distinct lack of aggrecan in the ECM and a pronounced intracellular localization of aggrecan within early and late chondrocytes (Figure 7). This suggested the cartilage derived from reprogrammed patient fibroblasts preserved the disease phenotype and showed the same aberrant aggrecan processing.

Aggrecan G3 domain plays a role in intracellular processing of the core protein and in facilitating its secretion [41]. Our observations of the chondrogenic behaviour of progenitor cells from FOCD-NS patients allow us to draw a number of conclusions about the cellular abnormalities associated with this mutation. It leads to retention of the aggrecan core within

the ER of chondrocytes and induces continued ER stress associated with an enlarged structure. This results in abnormal processing and assembly of the ECM, leading to rapid joint destruction and development of OA. This suggests that the mutation promotes a non-reversible cellular pathology during cartilage development.

ER dilation and ER stress, caused by mutations in ECM genes such as COMP, MATN3 and COL2A1, have been associated with the pathology of osteochondrodysplasias [42]. In the future, FOCD-NS iPSCs will be used to study the pathological roles associated with this G3 mutation in inducing ER stress, impacting cell behaviour and disturbing matrix regulation. In terms of development of therapy for FOCD-NS, these cells may be used in the development of drugs to restore cellular function or retard OA development. Furthermore, correction of the mutation in FOCD-NS-iPSCs using gene editing strategies may lead to a corrective cellular therapy for these patients.

Conclusion

In our current study, we have conducted research to investigate the molecular pathologies of FOCD-NS, which results in disproportionate growth, disturbed chondro-skeletal development and early onset OA.

Studying chondrocytes differentiated from patients' bone marrow mesenchymal stromal cells and iPSCs, we found large dysregulation and aberration in assembled extracellular matrix and irregulated cell fate, as consequences of endoplasmic reticulum stress, which was caused by an abnormal accumulation of mutated aggrecan protein.

Our observations reveal that cartilaginous tissue is the initial location where FOCD-NS developing, suggest that short stature found in FOCD-NS patients would be the sequel of

abnormal growth plate formation and regulation, moreover, show further evidence about the association between FOCD-NS and early onset OA.

These studies have provided us with a new insight into the cellular pathology of FOCD, a new model for studying the molecular mechanisms of osteochondrodysplasias and OA at early stage based on stem cell differentiation, and a new understanding for developing therapeutic approaches.

Acknowledgements

This study was funded by Science Foundation Ireland (SFI 09/SRC.B1794) and Irish Research Council (GOIPG/2014/96). This project has also received funding from the European Union's Seventh Framework Programme for research, technological development and demonstration under grant agreement no 223298. The authors sincerely thank the family members who participated in the study and Dr. Yelverton Tegner, Luleå Technical University, Luleå, Sweden for providing skin samples. The authors acknowledge the facilities and technical assistance of the Flow Cytometry Facility at the National University of Ireland Galway, a facility that is funded by NUIG and the Irish Government's Programme for Research in Third Level Institutions, Cycle5, National Development Plan 2007-2013. We thank Pierce Lalor, Dr. Kerry Thompson and the Centre for Microscopy & Imaging (www.imaging.nuigalway.ie) for assistance with TEM and confocal imaging, and Jingqiu Zhang (A*STAR Institute of Medical Biology, Singapore) for assistance with the iPSC reprogramming technique. We also thank Maggie Hall for helpful editing of the manuscript.

References

1. Edmonds EW, Polousky J. A review of knowledge in osteochondritis dissecans: 123 years of minimal evolution from Konig to the ROCK study group. Clin Orthop Relat Res. 2013;471:1118-1126.
2. Paget J. On the production of some of the loose bodies in joints. St Bartholomew's Hospital Reports 1870;6:1-4.
3. Schulz JF, Chambers HG. Juvenile osteochondritis dissecans of the knee: current concepts in diagnosis and management. Instr Course Lect. 2013;62:455-467.
4. Kosaka M, Nakase J, Takahashi R et al. Outcomes and failure factors in surgical treatment for osteochondritis dissecans of the capitellum. J Pediatr Orthop. 2013;33:719-724.
5. Preiss A, Heitmann M, Frosch KH. [Osteochondritis dissecans of the talus. Diagnosis and treatment]. Unfallchirurg. 2012;115:1099-1108; quiz 1109-1010.
6. Lunden JB, Legrand AB. Osteochondritis dissecans of the humeral head. J Orthop Sports Phys Ther. 2012;42:886.
7. Matsuda DK, Safran MR. Arthroscopic internal fixation of osteochondritis dissecans of the femoral head. Orthopedics. 2013;36:e683-686.
8. Hixon AL, Gibbs LM. Osteochondritis dissecans: a diagnosis not to miss. Am Fam Physician. 2000;61:151-156, 158.
9. Detterline AJ, Goldstein JL, Rue JP et al. Evaluation and treatment of osteochondritis dissecans lesions of the knee. J Knee Surg. 2008;21:106-115.
10. Andrew TA, Spivey J, Lindebaum RH. Familial osteochondritis dissecans and dwarfism. Acta Orthop Scand. 1981;52:519-523.
11. Phillips HO, Grubb SA. Familial multiple osteochondritis dissecans. Report of a kindred. J Bone Joint Surg Am. 1985;67:155-156.

12. Stattin EL, Tegner Y, Domellof M et al. Familial osteochondritis dissecans associated with early osteoarthritis and disproportionate short stature. Osteoarthritis Cartilage. 2008;16:890-896.

13. Stougaard J. FAMILIAL OCCURRENCE OF OSTEOCHONDRITIS DISSECANS. J Bone Joint Surg Br. 1964;46:542-543.

14. Stattin EL, Wiklund F, Lindblom K et al. A missense mutation in the aggrecan C-type lectin domain disrupts extracellular matrix interactions and causes dominant familial osteochondritis dissecans. Am J Hum Genet. 2010;86:126-137.

15. Wong-Palms S, Plaas AH. Glycosaminoglycan addition to proteoglycans by articular chondrocytes--evidence for core protein-specific pathways. Arch Biochem Biophys. 1995;319:383-392.

16. Kiani C, Chen L, Wu YJ et al. Structure and function of aggrecan. Cell Res. 2002;12:19-32.

17. Vertel BM, Walters LM, Grier B et al. Nanomelic chondrocytes synthesize, but fail to translocate, a truncated aggrecan precursor. J Cell Sci. 1993;104 (Pt 3):939-948.

18. Day JM, Murdoch AD, Hardingham TE. The folded protein modules of the C-terminal G3 domain of aggrecan can each facilitate the translocation and secretion of the extended chondroitin sulfate attachment sequence. J Biol Chem. 1999;274:38107-38111.

19. Day JM, Olin AI, Murdoch AD et al. Alternative splicing in the aggrecan G3 domain influences binding interactions with tenascin-C and other extracellular matrix proteins. J Biol Chem. 2004;279:12511-12518.

20. Murphy JM, Dixon K, Beck S et al. Reduced chondrogenic and adipogenic activity of mesenchymal stem cells from patients with advanced osteoarthritis. Arthritis Rheum. 2002;46:704-713.

21. Sullivan GJ, Hay DC, Park IH et al. Generation of functional human hepatic endoderm from human induced pluripotent stem cells. Hepatology. 2010;51:329-335.

22. Zhang L, Su P, Xu C et al. Chondrogenic differentiation of human mesenchymal stem cells: a comparison between micromass and pellet culture systems. Biotechnol Lett. 2010;32:1339-1346.

23. Ferrari D, Gong G, Kosher R et al. Chondrogenic Differentiation of hESC in Micromass Culture. In: Ye K, Jin S, eds. Human Embryonic and Induced Pluripotent Stem Cells: Humana Press; 2012:359-367.

24. Conroy PC, Saladino C, Dantas TJ et al. C-NAP1 and rootletin restrain DNA damage-induced centriole splitting and facilitate ciliogenesis. Cell Cycle. 2012;11:3769-3778.

25. Dockery P, Tidey RR, Li TC et al. A morphometric study of the uterine glandular epithelium in women with premature ovarian failure undergoing hormone replacement therapy. Hum Reprod. 1991;6:1354-1364.

26. Gillette MA, Carr SA. Quantitative analysis of peptides and proteins in biomedicine by targeted mass spectrometry. Nat Methods. 2013;10:28-34.

27. Zhang J, Lian Q, Zhu G et al. A human iPSC model of Hutchinson Gilford Progeria reveals vascular smooth muscle and mesenchymal stem cell defects. Cell Stem Cell. 2011;8:31-45.

28. Lee AS. The ER chaperone and signaling regulator GRP78/BiP as a monitor of endoplasmic reticulum stress. Methods. 2005;35:373-381.

29. Bonucci E. Bone mineralization. Front Biosci (Landmark Ed). 2012;17:100-128.

30. Balakrishnan L, Nirujogi RS, Ahmad S et al. Proteomic analysis of human osteoarthritis synovial fluid. Clin Proteomics. 2014;11:6.

31. Ea H-K, Nguyen C, Bazin D et al. Articular cartilage calcification in osteoarthritis: Insights into crystal-induced stress. Arthritis & Rheumatism. 2011;63:10-18.

32. Dominici M, Le Blanc K, Mueller I et al. Minimal criteria for defining multipotent mesenchymal stromal cells. The International Society for Cellular Therapy position statement. Cytotherapy. 2006;8:315-317.

33. Vincourt JB, Vignaud JM, Lionneton F et al. Increased expression of matrilin-3 not only in osteoarthritic articular cartilage but also in cartilage-forming tumors, and down-regulation of SOX9 via epidermal growth factor domain 1-dependent signaling. Arthritis Rheum. 2008;58:2798-2808.

34. Nakajima M, Kizawa H, Saitoh M et al. Mechanisms for asporin function and regulation in articular cartilage. J Biol Chem. 2007;282:32185-32192.

35. Sakao K, Takahashi KA, Arai Y et al. Asporin and transforming growth factor-beta gene expression in osteoblasts from subchondral bone and osteophytes in osteoarthritis. J Orthop Sci. 2009;14:738-747.

36. Tesche F, Miosge N. Perlecan in late stages of osteoarthritis of the human knee joint. Osteoarthritis Cartilage. 2004;12:852-862.

37. Chockalingam PS, Glasson SS, Lohmander LS. Tenascin-C levels in synovial fluid are elevated after injury to the human and canine joint and correlate with markers of inflammation and matrix degradation. Osteoarthritis Cartilage. 2013;21:339-345.

38. Vilim V, Olejarova M, Machacek S et al. Serum levels of cartilage oligomeric matrix protein (COMP) correlate with radiographic progression of knee osteoarthritis. Osteoarthritis Cartilage. 2002;10:707-713.

39. Chevalier X. Fibronectin, cartilage, and osteoarthritis. Semin Arthritis Rheum. 1993;22:307-318.

40. McMorrow JP, Crean D, Gogarty M et al. Tumor necrosis factor inhibition modulates thrombospondin-1 expression in human inflammatory joint disease through altered NR4A2 activity. Am J Pathol. 2013;183:1243-1257.

41. Zheng J, Luo W, Tanzer ML. Aggrecan synthesis and secretion. A paradigm for molecular and cellular coordination of multiglobular protein folding and intracellular trafficking. J Biol Chem. 1998;273:12999-13006.

42. Tsang KY, Chan D, Bateman JF et al. In vivo cellular adaptation to ER stress: survival strategies with double-edged consequences. J Cell Sci. 2010;123:2145-2154.

Figure legends

Figure 1. Characterization of control and FOCD-NS BM-MSCs. (A) Morphology of cultured mesenchymal cells isolated from control and FOCD-NS BM. Scale bars, 200 µm. (B) Flow cytometric analysis of control and FOCD-NS BM-MSCs for positive antigens CD90, CD73 and CD105 and negative markers CD11b, CD34, CD19, CD45 and HLA-DR. White histograms represent isotype controls and the grey overlay each antigen, percentage positive cells shown within histograms. (C) Adipogenic- and osteogenic- differentiation of control and FOCD-NS BM-MSCs. In adipogenic culture, phase contrast microscopy images show Oil Red-O positive cells,scale bars, 200 µm (left panels) and 100 µm (right panels). In osteogenic differentiation culture, mineralized nodules produced by osteoblasts were stained with Alizarin red. Scale bars, 100 µm.

Figure 2. Morphological and immunohistochemical analysis of in vitro chondrogenic differentiation using micropellet culture. Pellets were harvested at different time points (day 1, 3, 5, 7 and 14) (A) Representative stereo microscope images of overall morphology of chondrogenic pellets differentiated from control and FOCD-NS BM-MSCs. Scale bars, 1mm. (B) Toluidine blue staining on the sections of these pellets were shown. Scale bars,

500 µm. (C) Representative images of immunostained sections for aggrecan distribution. Scale bars, 500 µm. Insets are magnified images of the areas indicated by black arrows.

Figure 3. Morphological and immunohistochemical analysis of micromass cultures derived from control and FOCD-NS BM-MSCs. (A) Images showing the morphology of day 35 micromass cultures. Scale bar, 200 µm. (B) Confocal microscopy images showing double staining of aggrecan (red), GRP78 (green) and overlapping areas (yellow) on day 35 cultures. Cell nuclei stained with DAPI (blue). Scale bar, 50 µm.

Figure 4 Examination of ECM formation and chondrocytes status in micromass cultures derived from control and FOCD-NS BM-MSCs. (A) Quantification of GAG and DNA amounts in micromass cultures harvested at different time points. Average (± SD) ratios of GAG to DNA are shown. (B) Day 56 TEM images showed the distribution of protein fibres in ECM (a, c, d and f) and the ultrastructure of chondrotyes (b and e). The structure of rER is indicated by black arrows (b and e), with the corresponding magnified region shown bottom left in each case. The components of ECM in each group are showed in image c and f. Scale bar, 2 µm. (C) The volume fractions of rER to cell cytoplasm in these control and FOCD-NS sections are shown. (D) Immunostaining of collagen type II (appearing brown) in control (a) and FOCD-NS (b) sections from the day 42 cultures. Cell nuclei were stained with haematoxylin (blue). Scale bar, 500 µm.

Figure 5. Quantitative analysis of ECM proteins. ECM proteins in day 100 chondrogenic micromass cultures derived from healthy and FOCD-NS BM-MSCs were quantified using mass spectrometry. Three to six transitions for each protein were measured. The average amount of transition was calculated and normalized by the representative pellet volume to represent the corresponded protein. The mean ratio of protein expression of FOCD-NS to

control was calculated (n=3). A value lower than 1 means protein is down regulated in the patient sample.

Figure 6. Generation and characterization of iPSCs: includes FOCD-NS1-iPSC-2 (1), FOCD-NS1-iPSC-30 (2), FOCD-NS2-iPSC-9 (3) and FOCD-NS2-iPSC-13 (4). Normal iPSC line 33D-6 was the positive control ("+"). Skin fibroblasts obtained from FOCD-NS1 (5) and FOCD-NS2 (6) were included. (A) Reprogrammed fibroblasts underwent mesenchymal–epithelial transition at day 6 (a) and early iPSC like colony at day 14 (b) (see arrows; magnification 20x). Morphology of iPSCs colonies (magnification 10x) (c). (B) G-banding analysis showed normal karyotype in FOCD-NS-iPSCs. (C) RT-PCR data showing expression of retroviral transgenes (Tg) and endogenous pluripotent genes (Endo) in FOCD-NS-iPSCs. Non-template controls ("-") were performed in each PCR reaction. RNA extracted from retroviral infected 293T cells acted as positive controls for detection of Tg factors ("T"). (D) DNA sequencing confirming the aggrecan mutation in FOCD-NS-iPSCs (arrows). (E) Expression of pluripotency markers in FOCD-NS-iPSCs by immunostaining. Scale bar, 120 μm. (F) Flow cytometry analysis the expression of SSEA4. White histograms represent isotype controls and grey overlays SSEA4, percentage positive cells shown within histograms. (G) Histologic analysis of hematoxylin and eosin stained teratoma sections derived from iPSCs. Detected tissue types included: endoderm (top row), mesoderm (middle row) and ectoderm (bottom row). Black scale bar, 200 μm.

Figure 7. Verification of disease phenotype in iPSC-derived cartilage. Cartilage tissues in teratoma were positively stained with Safranin-O, shown as red (top row; scale bar, 500 μm). Aggrecan stained brown in teratoma cartilage from each iPSC line (middle row, scale

bar, 500 µm). Corresponding magnified images of aggrecan staining in teratoma cartilage (bottom row, scale bar 100 µm).

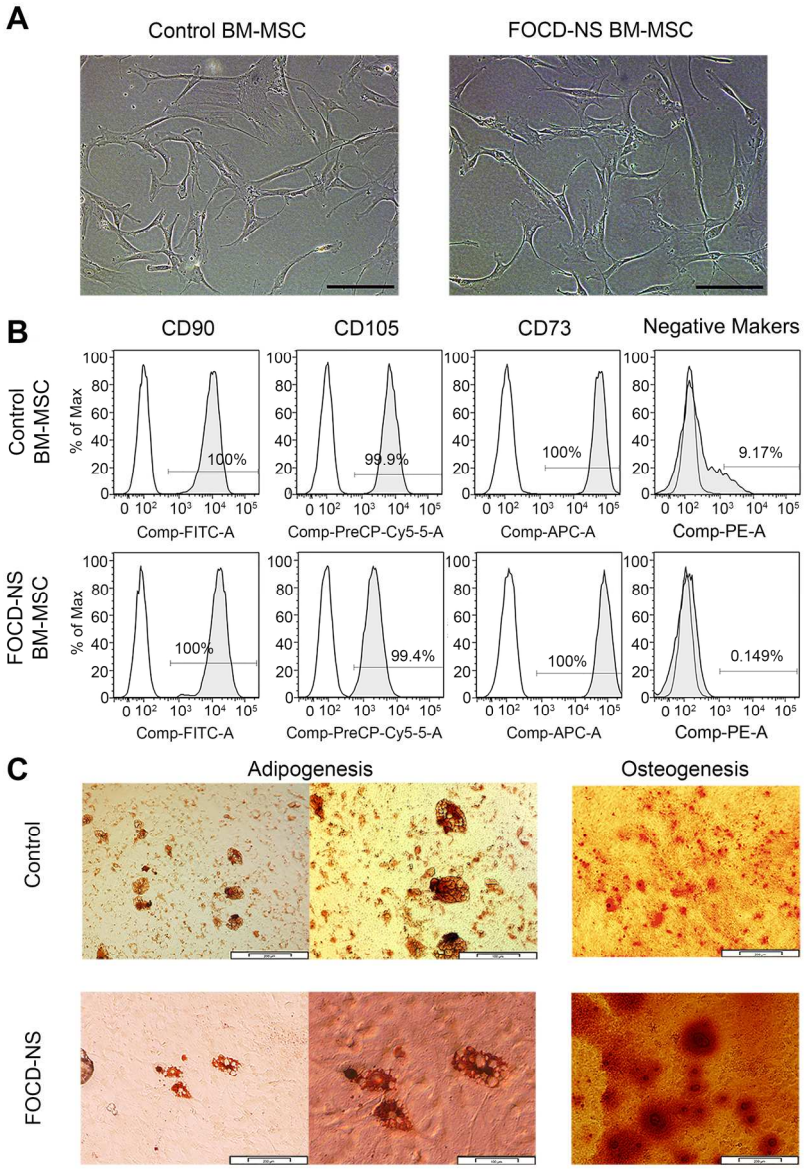

Figure 1. Characterization of control and FOCD-NS BM-MSCs. (A) Morphology of cultured mesenchymal cells isolated from control and FOCD-NS BM. Scale bars, 200 µm. (B) Flow cytometric analysis of control and FOCD-NS BM-MSCs for positive antigens CD90, CD73 and CD105 and negative markers CD11b, CD34, CD19, CD45 and HLA-DR. White histograms represent isotype controls and the grey overlay each antigen, percentage positive cells shown within histograms. (C) Adipogenic- and osteogenic- differentiation of control and FOCD-NS BM-MSCs. In adipogenic culture, phase contrast microscopy images show Oil Red-O positive cells,scale bars, 200 µm (left panels) and 100 µm (right panels). In osteogenic differentiation culture, mineralized nodules produced by osteoblasts were stained with Alizarin red. Scale bars, 100 µm.
161x238mm (300 x 300 DPI)

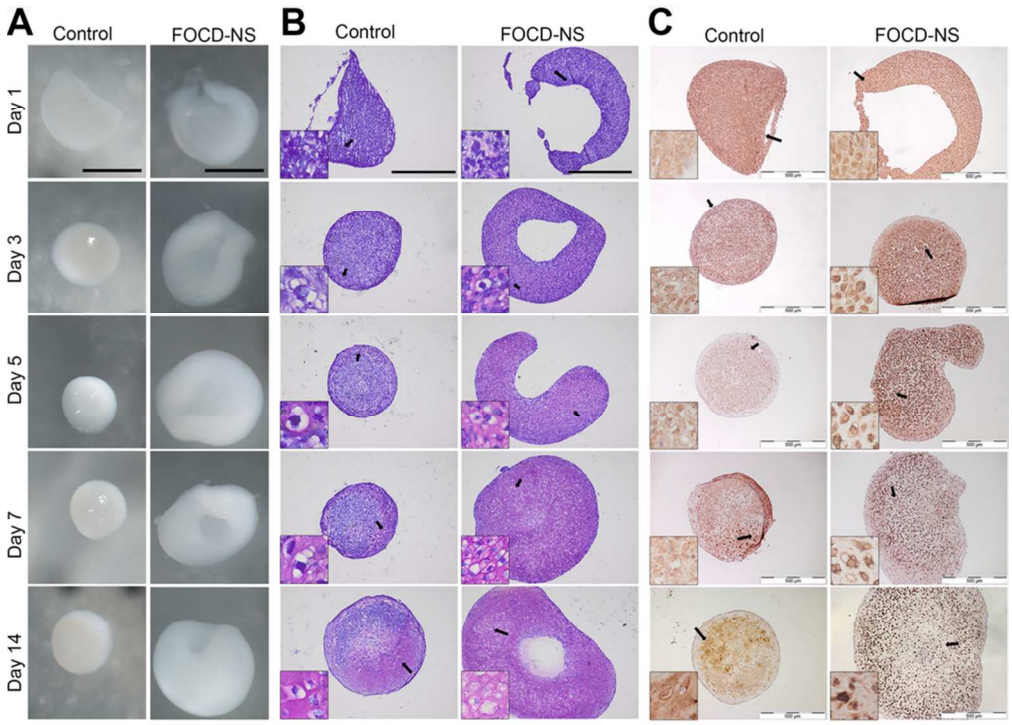

Figure 2. Morphological and immunohistochemical analysis of in vitro chondrogenic differentiation using micropellet culture. Pellets were harvested at different time points (day 1, 3, 5, 7 and 14) (A) Representative stereo microscope images of overall morphology of chondrogenic pellets differentiated from control and FOCD-NS BM-MSCs. Scale bars, 1mm. (B) Toluidine blue staining on the sections of these pellets were shown. Scale bars, 500 μm. (C) Representative images of immunostained sections for aggrecan distribution. Scale bars, 500 μm. Insets are magnified images of the areas indicated by black arrows.
81x58mm (300 x 300 DPI)

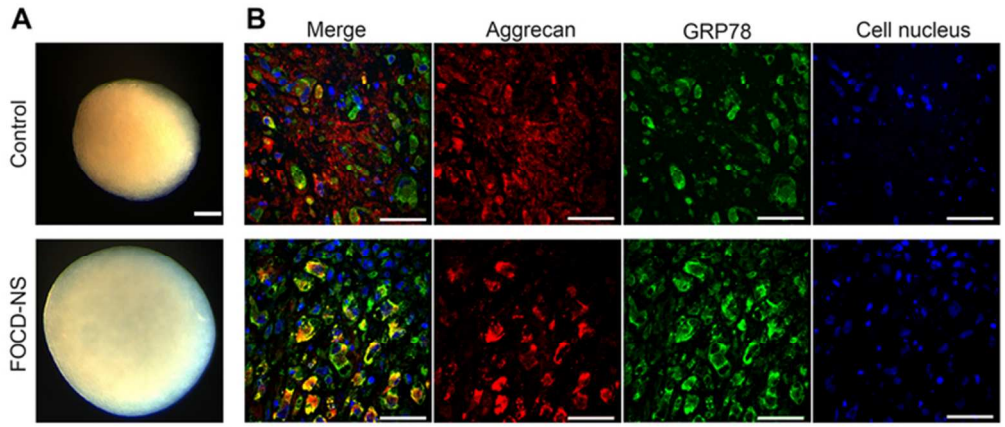

Figure 3. Morphological and immunohistochemical analysis of micromass cultures derived from control and FOCD-NS BM-MSCs. (A) Images showing the morphology of day 35 micromass cultures. Scale bar, 200 μm. (B) Confocal microscopy images showing double staining of aggrecan (red), GRP78 (green) and overlapping areas (yellow) on day 35 cultures. Cell nuclei stained with DAPI (blue). Scale bar, 50 μm.
63x27mm (300 x 300 DPI)

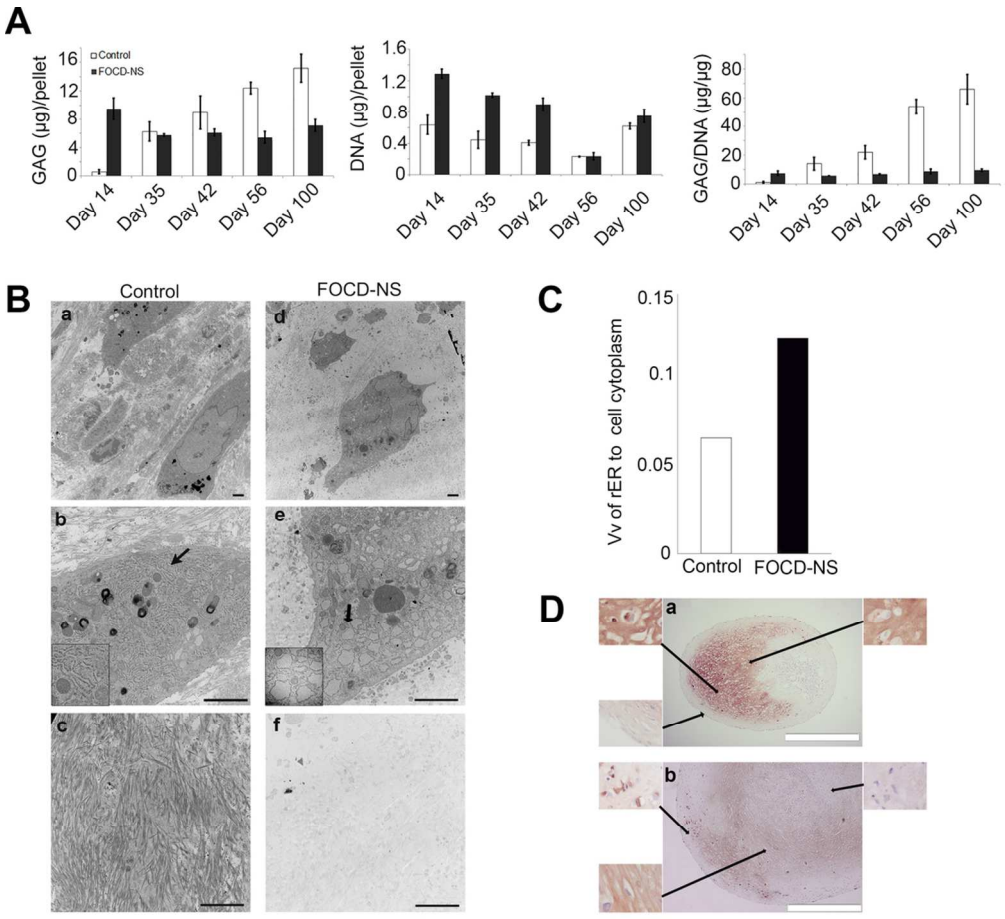

Figure 4 Examination of ECM formation and chondrocytes status in micromass cultures derived from control and FOCD-NS BM-MSCs. (A) Quantification of GAG and DNA amounts in micromass cultures harvested at different time points. Average (± SD) ratios of GAG to DNA are shown. (B) Day 56 TEM images showed the distribution of protein fibres in ECM (a, c, d and f) and the ultrastructure of chondrotyes (b and e). The structure of rER is indicated by black arrows (b and e), with the corresponding magnified region shown bottom left in each case. The components of ECM in each group are showed in image c and f. Scale bar, 2 μm. (C) The volume fractions of rER to cell cytoplasm in these control and FOCD-NS sections are shown. (D) Immunostaining of collagen type II (appearing brown) in control (a) and FOCD-NS (b) sections from the day 42 cultures. Cell nuclei were stained with haematoxylin (blue). Scale bar, 500 μm.
104x96mm (300 x 300 DPI)

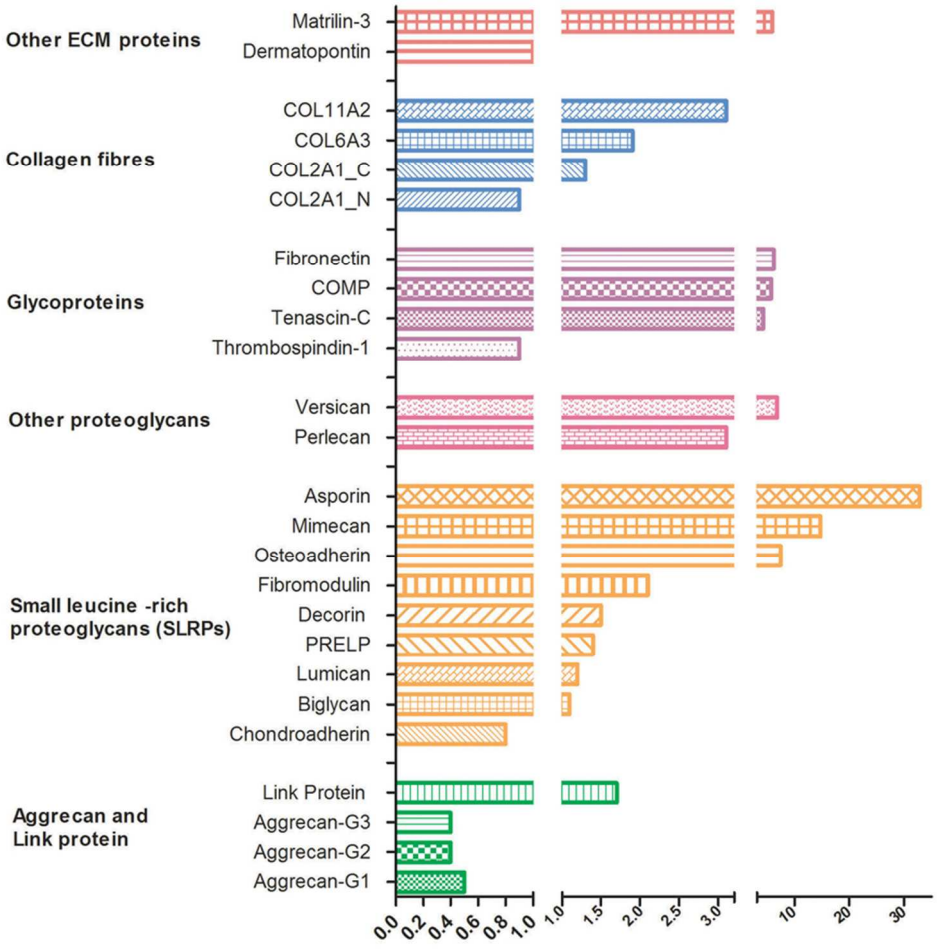

Figure 5. Quantitative analysis of ECM proteins. ECM proteins in day 100 chondrogenic micromass cultures derived from healthy and FOCD-NS BM-MSCs were quantified using mass spectrometry. Three to six transitions for each protein were measured. The average amount of transition was calculated and normalized by the representative pellet volume to represent the corresponded protein. The mean ratio of protein expression of FOCD-NS to control was calculated (n=3). A value lower than 1 means protein is down regulated in the patient sample.
78x76mm (300 x 300 DPI)

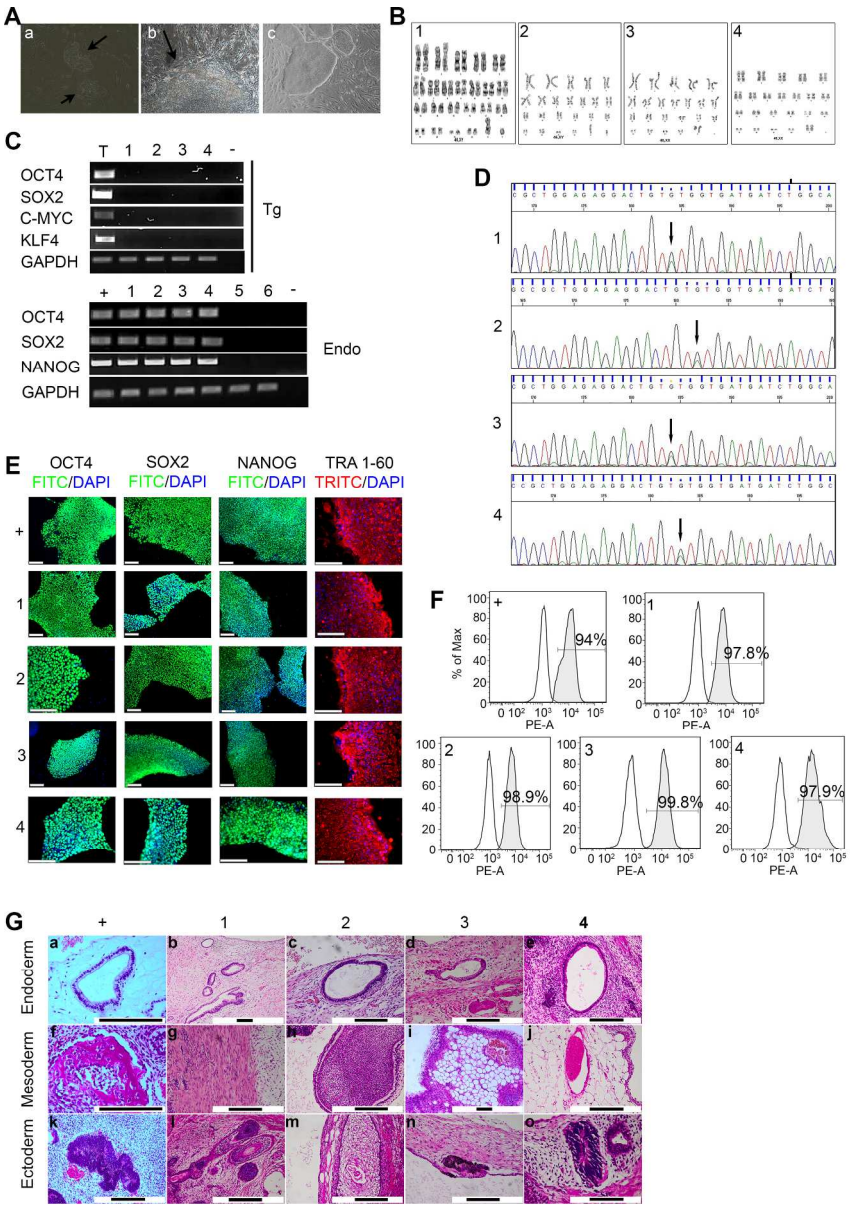

Figure 6. Generation and characterization of iPSCs: includes FOCD-NS1-iPSC-2 (1), FOCD-NS1-iPSC-30 (2), FOCD-NS2-iPSC-9 (3) and FOCD-NS2-iPSC-13 (4). Normal iPSC line 33D-6 was the positive control ("+"). Skin fibroblasts obtained from FOCD-NS1 (5) and FOCD-NS2 (6) were included. (A) Reprogrammed fibroblasts underwent mesenchymal–epithelial transition at day 6 (a) and early iPSC like colony at day 14 (b) (see arrows; magnification 20x). Morphology of iPSCs colonies (magnification 10x) (c). (B) G-banding analysis showed normal karyotype in FOCD-NS-iPSCs. (C) RT-PCR data showing expression of retroviral transgenes (Tg) and endogenous pluripotent genes (Endo) in FOCD-NS-iPSCs. Non-template controls ("-") were performed in each PCR reaction. RNA extracted from retroviral infected 293T cells acted as positive controls for detection of Tg factors ("T"). (D) DNA sequencing confirming the aggrecan mutation in FOCD-NS-iPSCs (arrows). (E) Expression of pluripotency markers in FOCD-NS-iPSCs by immunostaining. Scale bar, 120 µm. (F) Flow cytometry analysis the expression of SSEA4. White histograms represent isotype controls and grey overlays SSEA4, percentage positive cells shown within histograms. (G) Histologic analysis of hematoxylin and eosin stained teratoma sections derived from iPSCs. Detected tissue types included:

endoderm (top row), mesoderm (middle row) and ectoderm (bottom row). Black scale bar, 200 μm.
208x293mm (300 x 300 DPI)

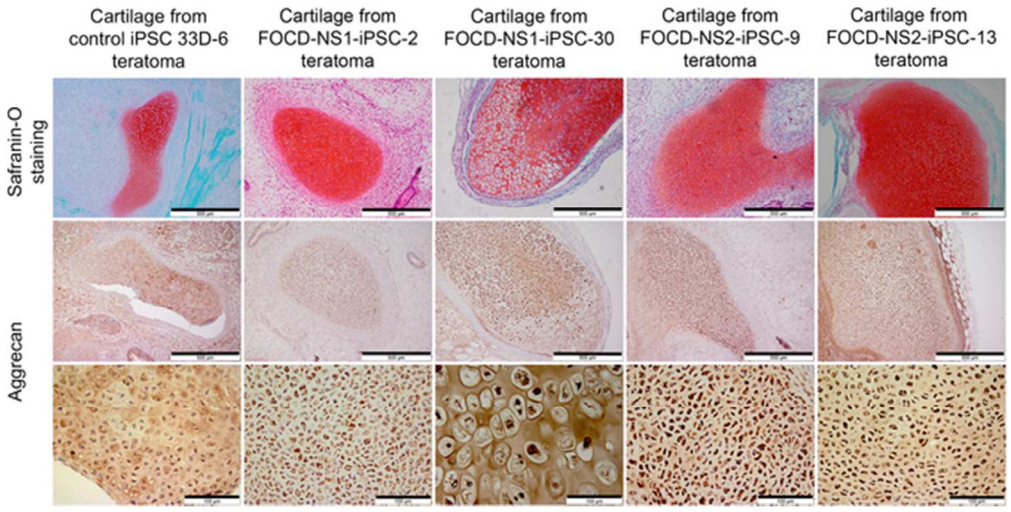

Figure 7. Verification of disease phenotype in iPSC-derived cartilage. Cartilage tissues in teratoma were positively stained with Safranin-O, shown as red (top row; scale bar, 500 μm). Aggrecan stained brown in teratoma cartilage from each iPSC line (middle row, scale bar, 500 μm). Corresponding magnified images of aggrecan staining in teratoma cartilage (bottom row, scale bar 100 μm).
56x28mm (300 x 300 DPI)

Chondrocytes derived from mesenchymal stromal cells and induced pluripotent cells of patients with familial osteochondritis dissecans exhibit an ER stress response and defective matrix assembly

Supplemental Data

Materials and Methods

Histological and immunohistochemical analysis of chondrogenic pellets. Chondrogenic pellets were fixed in 10% formalin for 2 hours at room temperature (RT). For immunohistochemical analysis, samples were processed by dehydration, paraffin embedding and sectioning. Paraffin sections (5 μm) were then deparaffinised and rehydrated. For detection of GAGs, sections were stained with 0.5% Toluidine blue (PH8) for 5 minutes at 60°C.

Immunohistochemistry was performed to investigate the distribution of collagen type II and aggrecan in chondrogenic pellets as described previously, with minor modifications [1]. For the detection of collagen type II, sections were treated with 4mg/ml Pepsin (Dako S3002) for 30 minutes at RT and for the detection of aggrecan, sections were incubated in 10mM sodium citrate (Sigma) pH 6.0 at 97°C for 20 minutes, followed by treatment with 40mU/ml chondroitinase ABC (Sigma) at 37°C for 30 minutes for antigen retrieval. Collagen type II and aggrecan were then detected using a biotin-streptavidin-peroxidase kit for mouse primary antibody (KPL) and employing a mouse anti-aggrecan antibody and a mouse anti-collagen type II antibody as primary antibodies at 4°C overnight. Signal was developed using diaminobenzidine (DAB) substrate kit (Abcam).

Multiple immunofluorescent staining of aggrecan and glucose regulated protein (GRP78) was performed to identify the intracellular location of aggrecan protein.

Sections were incubated with a premixed primary antibody solution, containing mouse anti-aggrecan antibody and rabbit anti-GRP78 antibody, at 4°C overnight followed by a premixed secondary antibody solution, containing Rhodamine (TRITC)-goat anti-mouse and DyLight 488-goat anti-rabbit for one hour at RT. Negative controls were performed with secondary antibody(s) only and detailed information of the antibodies used is listed in Supplementary Table 1.

Mass spectrometry analysis

For sample preparation, a modified protocol for extracting peptides from chondrogenic pellets derived from BM-MSCs was performed based on the previous description [2]. Briefly, three day 100 pellets per group, formed in micromass culture, were extracted with 100 µl of chaotropic extraction buffer (4M GdnHCl, 50mM sodium acetate, 100mM 6-aminocaproic acid, 5mM benzamidine, 5mM N-ethylmaleimide, pH 5.8) for 24h under gentle shaking at 4°C. The extract was obtained by centrifugation at 16,100 x g for 30 minutes. 50µl extract was reduced by 4mM dithiothreitol for 30 minutes at +56°C, alkylated by 16mM iodoacetamide for 60 minutes in the dark at room temperature, precipitated twice with ethanol and digested by 0.25µg trypsin gold (Promega, Madison, WI) in 0.1M ammonium bicarbonate (AMBIC) buffer pH 7.8 for 16 hours on a shaker at 37°C. After drying, samples were re-suspended in 100µl 0.5M AMBIC, run through 30kDa filter (PALL Life Sciences) and desalted with reversed-phase C18 columns (SEM SS04V-SS18V) according to the manufacturer's instructions (Nest Group,MA, USA). Targeted multiple reaction monitoring (MRM) analyses were performed using a LC-MS system comprising of a nano-LC (EasyTM, Thermo Scientific) and a triple quadrupole mass spectrometer (TSQ VantageTM, Thermo Scientific). Each sample was run in technical duplicate. The measured peptide transitions are listed in Supplementary

Table S3. Three to six transitions for each peptide were measured in a scheduled MRM method [2]. Briefly, the amount of each protein was normalized by the pellet volume. The mean ratios of ECM proteins between FOCD and control BM-MSC derived pellets were calculated.

Characterization of generated iPSCs

mRNA analysis. Total RNA was extracted from cells using RNeasy Mini Kit (Qiagen). RNA (1μg) was used for generation of complementary DNA using SuperScript III (Invitrogen). Reverse transcript (RT)-PCR was performed using OneTaq 2X Master Mix (BioLabs). Primer sequences for detection of retroviral reprogramming factors and endogenous pluripotent markers were as described previously [3]. Primer sequences are listed in Supplementary Table 2.

Immunocytochemistry. For immunocytochemistry, iPSCs were fixed with 4% paraformaldehyde for 10-20 minutes at RT. To detect intracellular markers, cells were treated with 0.5% saponin (Sigma) in PBS with/without 0.1% Triton X-100 (Sigma) for 10 minutes at RT. After blocking with 1% bovine serum albumin (Sigma) in PBS for 30 minutes at RT, cells were incubated with primary antibody overnight at 4°C. The primary antibodies used were against OCT-4, SOX2, NANOG and TRA 1-60. Secondary antibodies were applied for 1 hour at RT and cell nuclei labelled using Slow Fade Gold antifade reagent with DAPI (Invitrogen) with imaging by fluorescence microscopy. Detailed information of the antibodies used is listed in Supplementary Table 1.

Flow cytometry analysis. Cell preparation and fluorescent signal detection were as described in the section of Materials and Methods. Rat anti-SSEA4 conjugated with

PE was used to assess iPSCs with 0.17nM SYTOX (Invitrogen) for dead cell exclusion. Detailed information of antibodies used is listed in Supplementary Table 1.

Teratoma formation and tissue preparation. Cells for injection were prepared as described previously [3, 4]. Briefly, iPSCs were cultured to 90% confluence. Cell clumps were harvested by dispase treatment (Stemcell Technologies inc). After centrifugation at 200 x g for 5 minutes the cell pellet was resuspended in PBS with 30% Geltrex. 1-2 x 10^6 cells in 200µl were injected subcutaneously to the dorsal flank of SCID-Bergin mouse (Charles River). After 2 to 3 months, tumors were dissected and were fixed in 10% formalin overnight. Tissue was treated by decalcification solution (8N formic acid and 1N sodium formate, mixed at a 50:50 ratio) for 24 hours at RT, dehydrated, paraffin-embedded and 4 to 5µm sections were cut. Sections were stained with hematoxylin and eosin for histological analysis.

Karyotype analysis. For karyotype analysis, chromosomal spreads were prepared as previously described [5]. Briefly, iPSCs were treated with 0.1µg/ml colcemid (Invitrogen) for 2 hours at 37°C, 5% CO_2. Treated cells were harvested by incubation with accutase (Millipore). After centrifugation at 200 x g for 5 minutes, the cell pellet was resuspended in 75mM potassium chloride. The cell suspension was gently pipetted to break down remaining cell clumps and incubated for 20 minutes at 37°C prior to fixation in ice cold fixative solution containing methanol and acetic acid (3:1). Standard G-banding chromosome analysis was performed at The Doctors Laboratory (TDL), London.

Mutation validation. Genomic DNA was extracted from cells using DNeasy Blood & Tissue Kits (Qiagen). Primer sequences to amplify exon 17 of ACAN were as described previously [6]. PCR products were purified by Gel Extraction Kit (Qiagen).

For sequence analysis, samples were sent to Eurofins MWG Operon (Germany) and results were analysed by Sequence Scanner Version: 1.0 software (Applied Biosystems). Primer sequences are listed in Supplementary Table 2.

Supplemental Figure legend

Supplemental Figure 1: Ultra-structural analysis of the distribution of protein fibres from control and FOCD-NS sample. Pellets from both groups were formed in micromass culture and harvested at day 56. Images of different areas between the edge and centre of each control and FOCD-NS pellet allow comparison of the ECM components. Scale bar, 2 μm.

Supplemental References

1. Murphy JM, Dixon K, Beck S et al. Reduced chondrogenic and adipogenic activity of mesenchymal stem cells from patients with advanced osteoarthritis. Arthritis Rheum. 2002;46:704-713.
2. Gillette MA, Carr SA. Quantitative analysis of peptides and proteins in biomedicine by targeted mass spectrometry. Nat Methods. 2013;10:28-34.
3. Takahashi K, Tanabe K, Ohnuki M et al. Induction of pluripotent stem cells from adult human fibroblasts by defined factors. Cell. 2007;131:861-872.
4. Ohnuki M, Takahashi K, Yamanaka S. Generation and characterization of human induced pluripotent stem cells. Curr Protoc Stem Cell Biol. 2009;Chapter 4:Unit 4A 2.
5. Campos PB, Sartore RC, Abdalla SN et al. Chromosomal spread preparation of human embryonic stem cells for karyotyping. J Vis Exp. 2009.

6. Stattin EL, Wiklund F, Lindblom K et al. A missense mutation in the aggrecan C-type lectin domain disrupts extracellular matrix interactions and causes dominant familial osteochondritis dissecans. Am J Hum Genet. 2010;86:126-137.

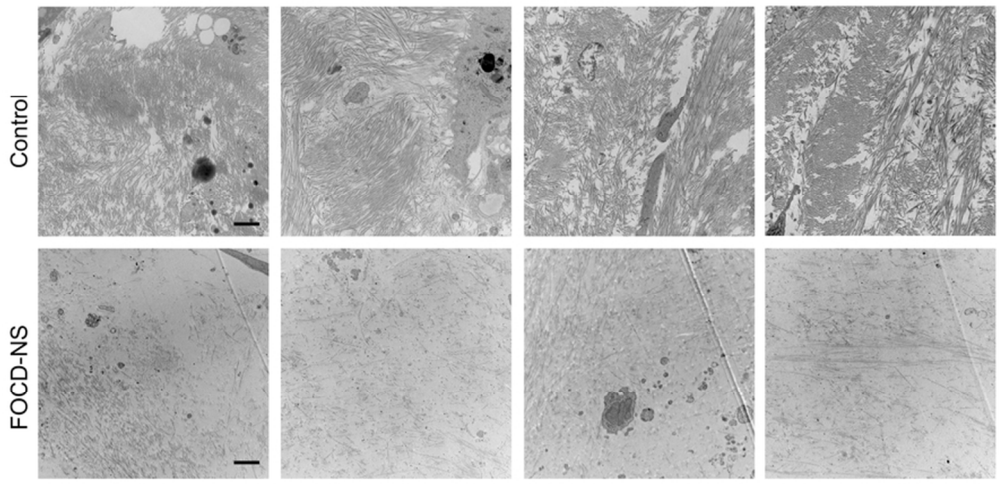

Supplemental Figure 1: Ultra-structural analysis of the distribution of protein fibres from control and FOCD-NS sample. Pellets from both groups were formed in micromass culture and harvested at day 56. Images of different areas between the edge and centre of each control and FOCD-NS pellet allow comparison of the ECM components. Scale bar, 2 µm.
75x36mm (300 x 300 DPI)

Supplemental Table 1: Antibodies information

Antibody	Dilution	Supplier (Cat. number)
Aggrecan	1:100	Abcam (ab3778)
GRP78/Bip	1:100	Abcam (ab21685)
OCT4	1:100	Cell Signaling (#9656)
SOX2	1:100	Cell Signaling (#9656)
NANOG	1:100	Cell Signaling (#9656)
TRA1-60	1:100	Cell Signaling (#9656)
Anti-mouse IgG (H+L), F(ab')2 Fragment (Alexa Fluor® 555 Conjugate)	1:200	Cell Signaling (#4409S)
Anti-rabbit IgG (H+L), F(ab')2 Fragment (Alexa Fluor® 488 Conjugate)	1:200	Cell Signaling (#4412S)
HistoMark Goat anti-Mouse IgG (H+L), Biotin	Ready to use reagent	KPL (71-00-18)
MSCs analysis kit		*BD* Biosciences (562245)
SSEA4	1:150	*BD* Biosciences (560128)

Supplemental Table 2: Primer sequences

Target gene	Forward primer	Reverse primer
Endo OCT4	GACAGGGGGAGGGAGGAGCTAGG	CTTCCCTCCAACCAGTTGCCCCAAAC
Endo SOX2	GGGAAATGGGAGGGGTGCAAAAGAGG	TTGCGTGAGTGTGGATGGGATTGGTG
Endo NANOG	CAGCCCCGATTCTTCCACCAGTCCC	CGGAAGATTCCCAGTCGGGTTCACC
Tg OCT4	CCCCAGGGCCCCATTTTGGTACC	CCCTTTTTCTGGAGACTAAATAAA
Tg SOX2	GGCACCCCTGGCATGGCTCTTGGCTC	TTATCGTCGACCACTGTGCTGCTG
Tg KLF4	ACGATCGTGGCCCCGGAAAAGGACC	TTATCGTCGACCACTGTGCTGCTG
Tg C-MYC	CCACAACCGAAAATGCACCAGCCCCAG	TTATCGTCGACCACTGTGCTGCTG
Aggrecan exon17	ATTCCCAGCAGTTTTTGTGC	GATCCTATCCTCCCCTGACC
GAPDH	GCTGGAGCTGGATCGGAAGCACAT	CGATGCAGCGCAGGAAGACAT

Supplemental Table 3: List of the measured peptide transitions for ECM proteins measured by MRM analysis and the ratio of patients' to controls' (n=3)

Protein Name	Accession No.	Peptide Sequence	Peptide fold change	Protein fold **change**
Asporin	Q9BXN1	LYLSHNQLSEIPLNLPK	44.0	32.8
		ISTVELEDFK	*	
		SLYSAISLFNNPVK	*	
		YWEMQPATFR	21.6	
Mimecan	P20774	ESAYLYAR	8.6	14.8
		LSLLEELSLAENQLLK	24.5	
		LEGNPIVLGK	11.3	
Osteoadherin	Q99983	IDYGVFAK	7.3	7.5
		LLLGYNEISK	7.8	
Versican core protein	P13611	LLASDAGLYR	6.3	6.8
		LATVGELQAAWR	7.3	
Fibronectin	P02751	WLPSSSPVTGYR	9.1	6.3
		YEVSVYALK	4.1	
		SYTITGLQPGTDYK	5.8	
Matrilin-3	O15232	IIDTLDIGPADTR	6.0	6.0
		VAVVNYASTVK	7.1	
		AQASGIELYAVGVDR	5.0	
Cartilage oligomeric matrix protein	P49747	ELQETNAALQDVR	6.9	5.8
		DTDLDGFPDEK	5.7	
		LVPNPGQEDADR	5.9	
		SSTGPGEQLR	4.6	
Tenascin-C	P24821	GLEPGQEYNVLLTAEK	4.4	4.4
		AYAAGFGDR	3.4	
		EEFWLGLDNLNK	5.5	
		ITAQGQYELR	4.2	
Collagen alpha-2(XI) chain	P13942	DFSLLTVVR	3.0	3.1
		FLYEDQTGRPQPPSQPVFR	3.2	
Perlecan	P98160	EVSEAVVDTLESEYLK	3.3	3.1
		LEGDTLIIPR	2.6	
		IAHVELADAGQYR	3.4	
Fibromodulin	Q06828	YLPFVPSR	1.7	2.1

		ELHLDHNQISR	2.0		
		IPPVNTNLENLYLQGNR	2.0		
		SAMPADAPLCLR	2.7		
Collagen alpha-3(VI) chain	P12111	SLDEISQPAQELK	1.8	1.9	
		SDDEVDDPAVELK	1.6		
		LSDAGITPLFLTR	2.2		
Hyaluronan and proteoglycan link protein 1	P10915	DPTAFGSGIHK	1.3	1.7	
		FYYLIHPTK	2.7		
		VGQIFAAWK	1.1		
Decorin	P07585	VVQCSDLGLDK	1.6	1.5	
		NLHALILVNNK	1.2		
		VSPGAFTPLVK	1.7		
Proline-arginine-rich end leucine-rich repeat protein	P51888	NQLEEVPSALPR	1.3	1.4	
		LENLLLLDLQHNR	2.2		
		VPTAIHQLYLDSNK	0.7		
Lumican	P51884	SLEDLQLTHNK	1.2	1.2	
		ISNIPDEYFK	1.1		
		FNALQYLR	1.3		
Biglycan	P21810	VVQCSDLGLK	1.0	1.1	
		IQAIELEDLLR	1.5		
		LGLGHNQIR	1.0		
		VPSGLPDLK	0.9		
Collagen alpha-1(II) chain N-propeptide	P02458	GPPGPQGPAGEQGPR	0.9	1.1	
Collagen alpha-1(II) chain chondrocalcin	P02458	SLNNQIESIR	1.3		
Dermatopontin	Q07507	GATTTFSAVER	1.0	1.0	
Thrombospondin-1	P07996	GPDPSSPAFR	0.7	0.9	
		SITLFVQEDR	0.8		
		FVFGTTPEDILR	1.2		
Chondroadherin	O15335	NQLSSYPSAALSK	0.7	0.8	
		SIPDNAFQSFGR	0.6		
		YLETLWLDNTNLEK	1.1		
		FSDGAFLGVTTLK	0.7		
Aggrecan core protein G1 domain	P16112	VSLPNYPAIPSDATLEVQSLR	1.3	0.7	0.5
		GIVFHYR	0.5		

		YTLDFDR	0.4	
Aggrecan core protein G2 domain	P16112	YPIVSPR	0.4	0.4
		LEGEVFFATR	0.4	
Aggrecan core protein G3 domain	P16112	ETWVDAER	0.4	0.4
		TIEGDFR	0.3	
		YEINSLVR	0.4	
			*	*
Cartilage intermediate layer protein 2	Q8IUL8	TTDWALPSAVGE R		
		VVAADSGEPLR	*	
		DLTSAASAPSDLR	*	
		FVDSDGELAPLR	*	
		VFLVGNVEIR	*	
		IQGPQEYMVR	*	
		LLESPATALGDIR	*	
		EMSEAAQAQAR	*	

(Note: Proteins marked with (*) were only detected in FOCD-NS pellets but not in control pellets.)

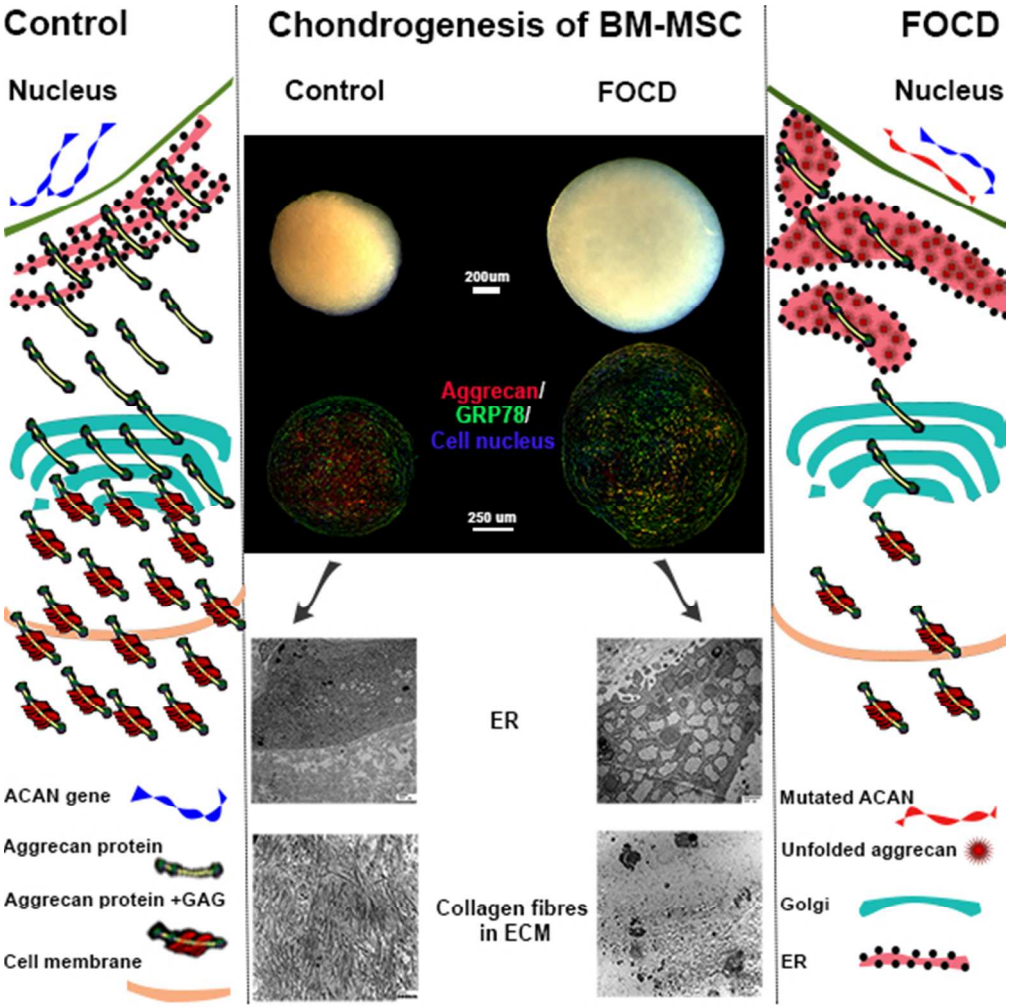

50x50mm (300 x 300 DPI)

Graphical abstract legend:

Patients with familial osteochondritis dissecans (FOCD) carry a heterozygous mutation in the ACAN gene, which results in a Val-Met replacement in the C-type lectin domain of aggrecan protein. Studying a stem cell-derived FOCD chondrogenic model, we found the mutation resulted in unfolded aggrecan protein which accumulated in the endoplasmic reticulum (ER). The overloaded ER influenced the function of FOCD chondrocytes and lead to defective extracellular matrix (ECM) formation. Disease phenotype has been validated with FOCD models derived from bone marrow-derived mesenchymal stromal cells (BM-MSCs) and induces pluripotent stem cells (iPSCs).